Applied Surface Science 270 (2013) 519–525

Contents lists available at SciVerse ScienceDirect

Applied Surface Science

journal homepage: www.elsevier.com/locate/apsusc

Microstructure and properties of duplex (Ti:N)-DLC/MAO coating on magnesium alloy

Wei Yang[a], Peiling Ke[a], Yong Fang[b], He Zheng[a], Aiying Wang[a,*]

[a] Ningbo Key Laboratory of Marine Protection Materials, Ningbo Institute of Materials Technology and Engineering, Chinese Academy of Sciences, Ningbo 315201, China
[b] Sir Run Run Shaw Hospital, School of Medicine, Zhe Jiang University, Zhejiang 310016, China

ARTICLE INFO

Article history:
Received 23 October 2012
Received in revised form 8 January 2013
Accepted 12 January 2013
Available online 20 January 2013

Keywords:
AZ80 Mg alloy
Microarc oxidation
(Ti:N)-DLC top film
Microstructure
Properties

ABSTRACT

Ti and N co-doped diamond-like carbon ((Ti:N)-DLC) film was deposited on the MAO coated substrate using a hybrid beam deposition system, which consists of a DC magnetron sputtering of Ti target and a linear ion source (LIS) with C_2H_2 and N_2 precursor gas. The microstructure and properties of the duplex (Ti:N)-DLC/MAO coating were investigated. Results indicate that the (Ti:N)-DLC top film with TiN crystalline phase was formed. Ti and N co-doping resulted in the increasing I_D/I_G ratio. The significant improvement in the wear and corrosion resistance of duplex (Ti:N)-DLC/MAO coating was mainly attributed to the increased binding strength, lubrication characteristics and chemical inertness of (Ti:N)-DLC top film. The superior low-friction and anti-corrosion properties of duplex (Ti:N)-DLC/MAO coating make it a good candidate as protective coating on magnesium alloy.

1. Introduction

Magnesium and its alloys are increasingly used in the automotive industry because of the flexibility in fabrication and high strength-to-weight ratio [1]. Unfortunately, their practical applications have been limited due to the poor wear and corrosion resistance [2]. One of the effective ways to overcome these drawbacks is to coat a protective layer with high wear and corrosion resistance. Recently, microarc oxidation (MAO), a simple and novel surface technique, has been widely used to prepare ceramic oxide coatings, having relatively high hardness and excellent adhesion strength, on the surfaces of valve metals and their alloys, e.g., Al, Mg, Ti, etc. [3–6]. However, such MAO coatings on magnesium alloy often exhibited a relatively high friction coefficient against many counter materials during the dry sliding processing, and also suffered from corrosion failure due to the micropores distributed on the coating surface [7–10]. Therefore, a design of duplex treatment combined MAO and a low friction layer was considered in this work.

As diamond-like carbon (DLC) film is well known for its high hardness, low friction, excellent wear resistance and chemical innerness, it may be able to counterbalance the disadvantages of magnesium alloy [11,12]. For such DLC film/substrate system, the key breakthrough is its weak adhesion to the soft substrate because of the mechanical incapability and high internal stress [13–15]. The previous study has proven that metal film as an interlayer or metal doping could significantly improve the adhesion of DLC film to the magnesium substrate [16–19]. However, these coatings had a poor corrosion resistance due to the existence of through-thickness defects in the films and the large difference between interlayer and the Mg substrate in galvanic series [20–22].

Our previous work demonstrated that the MAO coating as a interlayer of DLC film could significantly improve the corrosion and wear resistance of the Mg substrate, which was attributed to the restrained corrosion process between the interlayer and substrate for the thick MAO coating and a low friction coefficient of DLC top thin film [23]. Meanwhile, metal doping seems a potential method to further improve the properties of DLC film efficiently [21].

Based on the above consideration, in this work, Ti and N co-doping is employed to form the DLC film with TiN crystalline phase on the MAO coating surface, which is expected to increase the binding force. Otherwise, the corrosion process induced by the doping metal (such as Ti) may be restrained due to the formation of TiN crystalline phase in the DLC film. In addition, it is known that TiN has the high thermal stability. If the microstructure of DLC film with TiN crystalline phase was formed, it might increase the thermal stability of the coating, which could further improve its tribological properties [24]. Subsequently, in this study, the microstructure, tribological and corrosive properties of the duplex (Ti:N)-DLC/MAO coated AZ80 Mg alloy are systematically investigated.

2. Experimental procedure

The AZ80 Mg alloy substrate (mass fraction: Al 7.8–9.2%, Mn 0.15–0.5%, Zn 0.2–0.8%, Mg balance) discs (Φ20 mm × 5 mm)

* Corresponding author. Tel.: +86 574 86685170; fax: +86 574 86685159.
E-mail addresses: aywang@nimte.ac.cn, yangwei_smx@nimte.ac.cn (A. Wang).

0169-4332/$ – see front matter.
http://dx.doi.org/10.1016/j.apsusc.2013.01.073

Table 1
Surface roughness and thickness of the coatings.

Films	Thickness/nm	Ra/nm
DLC	480.4	0.92
Ti-DLC	556.4	1.87
(Ti:N)-DLC	500.6	2.69

were mechanically polished to an average surface roughness of Ra ≈ 23.5 nm, followed by ultrasonic cleaning in acetone for 20 min. The fabrication of the duplex MAO/(Ti:N)-DLC coatings on AZ80 Mg alloy discs was performed by two steps including MAO and ion beam deposition technique. In MAO preparation, the ceramic coating was fabricated in an aqueous solution containing 5 g/L sodium silicate (Na_2SiO_3), 10 g/L potassium hydroxide (KOH), and 8 g/L potassium fluoride (KF), by a constant voltage mode on a direct-current (DC) pulsed electrical source with the frequency of 500 Hz and the duty cycle of 5%. The oxidation time was 3 min and the thickness of ceramic coating was 5 μm. The DLC, Ti-DLC and (Ti:N)-DLC top films were prepared on the MAO coated samples and Si substrates by a hybrid ion beam deposition system (including a linear ion source (LIS) and a magnetron sputtering source) as shown in the literature [25]. The base pressure was evacuated to a vacuum of 2×10^{-5} Torr. Hydrocarbon gas (C_2H_2) and N_2 (C_2H_2/N_2 ratio 8 sccm:7 sccm) were introduced into the linear ion source to obtain the hydrocarbon ions for (Ti:N)-DLC deposition. The Ar sputtering gas was supplied to the magnetron sputter for Ti doping, as the sputtering current of 2.5 A and Ar flux of 70 sccm. Typical values of LIS voltage and current were 1100 ± 20 V and 0.15 A, respectively. The DC power supplied to the sputtering gun was about 1050 W (420 V, 2.5 A). The C_2H_2/Ar ratio was controlled at 15 sccm:70 sccm as the Ti-DLC film was deposited. The DLC film was deposited as the C_2H_2 gas flux was 15 sccm. A negative pulsed bias voltage of −100 V was applied to the substrate. The deposition time was 40 min. The surface roughness and thickness of the films are summarized in Table 1.

The surface morphology of the duplex coating was examined using atomic force microscopy (AFM) and field emission scanning electron microscope (FESEM). Energy dispersive X-ray spectrometer (EDS) was used to test the element distribution of the coatings after friction tests. Raman spectroscopy with an incident Ar^+ beam at a wavelength of 514.5 nm was used to measure the atomic bonds of films. An X-ray photoelectron spectroscopy (XPS) with Al (mono) Kα irradiation at pass energy of 160 eV was used to characterize the chemical bonds of the films. The binding energies were referenced to the C 1s line at 285.0 eV. High-resolution transmission electron microscopy of the films was performed on Tecnai F20 electron microscope operated at 200 keV with a point-to-point resolution of 0.24 nm. The TEM specimens were prepared by peeling off the films from the NaCl crystalline substrates, which were dissolved in deionized water. The adhesion of the films to the AZ80 substrates was assessed by a scratch tester performed on a Rockwell diamond indenter with a conical tip of 0.2 mm in radius. The normal load of the indenter was linearly ramped from the minimum to the maximum during scratching. Here, the minimum load and the maximum load were 1 N and 15 N, respectively. In the test, the scratch length was 3.00 mm and the scratch speed was 0.2 mm/s. The wear resistance of the coated samples was assessed using ball-on-disk wear tests. During the tests, a 1 N contact load was applied on the samples through a steel ball (SUJ-2, HRC60) with a diameter of 6 mm. The samples (discs) were tested when they rotated at a constant speed of 0.1 m/s. The diameter of the sliding track was 2 mm. For the electrochemical investigation, the experiments were performed on an Autolab Pgstat302 advanced electrochemical system, using the conventional three-electrode technique. The coated sample was masked by epoxy resin with the surface area of 0.5 cm^2 exposed in 3.5 wt.% NaCl solution. These tests were carried out at 1 mV/s at room temperature.

3. Results and discussion

3.1. Coating characteristics

The bonding natures of samples were investigated using XPS analysis. Fig. 1(a) shows the deconvolution of N 1s peak of the (Ti:N)-DLC top film, giving two peaks at 396.6, 398.3 and 400.4 eV, which are assigned to TiN, —N= and C—N bonds, respectively [26,27]. The deconvolution of Ti $2p_{3/2}$ and Ti $2p_{1/2}$ peaks of (Ti:N)-DLC top film was shown on Fig. 1(b), which gives four peaks at 455.481, 457.581, 461.20 and 463.46 eV. For the deconvolution of Ti $2p_{3/2}$ peak, it gives two peaks at 455.481 and 457.581 eV, which are assigned to TiN and TiO_2 bonds. The deconvolution of Ti $2p_{1/2}$ peak also gives two peaks at 461.20 and 463.46 eV, which are also assigned to TiN and TiO_2 bonds. So it can be deduced that TiN was formed in the (Ti:N)-DLC film. Furthermore, the microstructure of this film is analyzed by TEM. Fig. 2 shows the plan-view TEM images and corresponding sectional area electron diffraction (SAED) patterns of the (Ti:N)-DLC film. It is different from the pattern of the pure DLC film representing the typical amorphous structure [21]. The crystalline diffraction ring-like are observed in Fig. 2(b), which is different from the pattern of pure DLC film representing the typical amorphous structure [21]. Those rings could be identified to be the (2 0 0) and (2 2 0) reflections of the face-centered (FCC) titanium nitride structure with the interplanar spacings of 0.213 nm

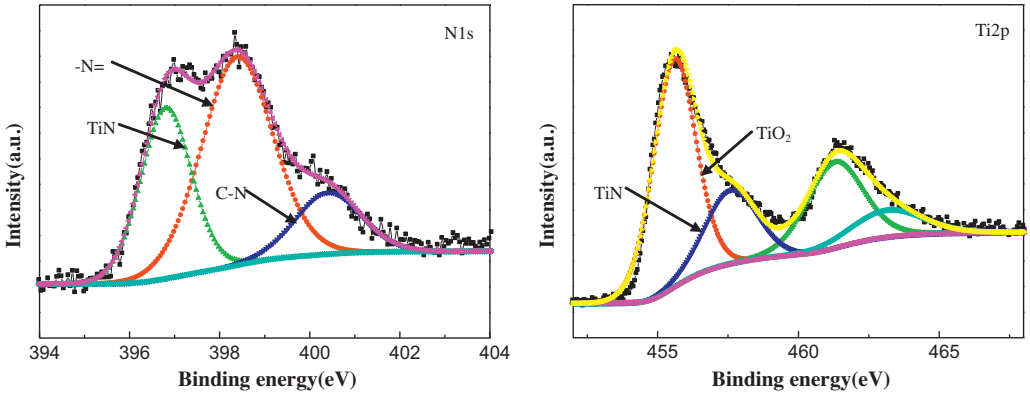

Fig. 1. Typical N 1s and Ti 2p high-resolution XPS spectras of the (Ti:N)-DLC film. (For interpretation of the references to color in figure legend, the reader is referred to the web version of the article.)

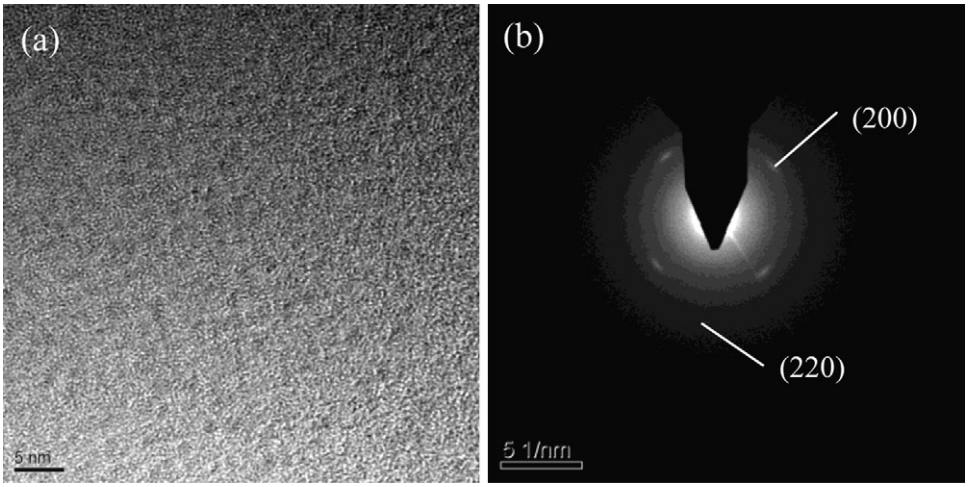

Fig. 2. (a) Typical TEM micrograph and (b) corresponding diffraction pattern of the (Ti:N)-DLC film.

and 0.149 nm, which implies that the TiN crystalline phase formed in the carbon film.

Usually, the Raman spectra of DLC films can be fitted using two Gaussians peaks, the G peak at approximately 1540 cm^{-1} and the D peak at approximately 1345 cm^{-1}, as shown in the insert figure of Fig. 3. It is known that the G peak is due to the bond stretching of all pairs of sp^2 bond in both aromatic rings and carbon chains, and D peak is due to the breathing modes of sp^2 bond only in rings [28,29]. Fig. 4 shows the dependencies of the G-peak position and the intensity ratio of the position of the peaks as a function of the coating styles. According to the G peak position and the intensity ratio of D peak to G peak (I_D/I_G), the sp^2/sp^3 ratio of the DLC, Ti-DLC and (Ti:N)-DLC films can be characterized [30]. It should be noted that G peak position and I_D/I_G ratio increase as the Ti and N co-doping into the DLC film, implying the increased sp^2/sp^3 ratio for (Ti:N)-DLC top film [31,32].

Fig. 5 shows the surface morphologies of the MAO, DLC/MAO, Ti-DLC/MAO and (Ti:N)-DLC/MAO coatings on magnesium alloy. Fig. 5(a) shows that the MAO coating is characterized by a large number of micropores with different apertures, which corresponds to the growth mechanism of MAO coating during the oxidation process. It also can be seen that the coating surface is smooth and dense without some condensation products heap disorderly around the holes, which attributes to the MAO processing parameter for decreasing the breakdown potential of ceramic coating. In the case of the DLC/MAO, Ti-DLC/MAO and (Ti:N)-DLC/MAO coatings, it can be obtained that the duplex coatings are not uniform, and some micropores, which are inherent in the surface of MAO coating, are still observed on the coating surface. Compared with the MAO coating, the aperture of micropores on the coating surface decreases due to the interstitial filling of top DLC, Ti-DLC and (Ti:N)-DLC films, which indicates that it is useful to increase the binding strength between coating and substrate.

Fig. 6 shows the critical loads of the coated samples in the scratch test in this study. For the MAO/AZ80, DLC/MAO/AZ80 and Ti-DLC/MAO/AZ80 and (Ti:N)-DLC/MAO/AZ80 systems, the critical loads of the MAO coating was 7.44 N. It was slightly higher than the duplex DLC/MAO and Ti-DLC/MAO coatings, which can be deduced that the critical loads of the three duplex coatings were determined by the metallurgical bonding at the interface created by MAO treatment. It can be also obtained that with Ti doping or (Ti:N) doping, the critical loads of the duplex Ti-DLC/MAO and (Ti:N)-DLC/MAO coatings were improved than that of DLC/MAO, which attributes to the addition of Ti or N atoms into the DLC film for the residual stress release [33]. As a result, the duplex (Ti:N)-DLC/MAO coating exhibited the highest critical load, which was very useful to improve the tribological behavior of the coated sample.

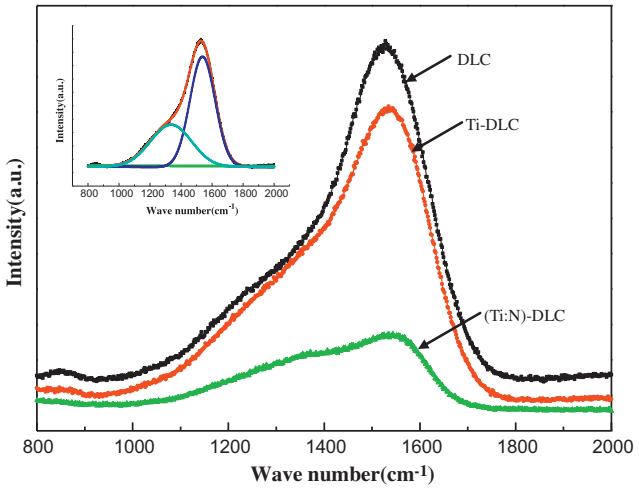

Fig. 3. Raman spectra of the DLC, Ti-DLC and (Ti:N)-DLC films. (For interpretation of the references to color in figure legend, the reader is referred to the web version of the article.)

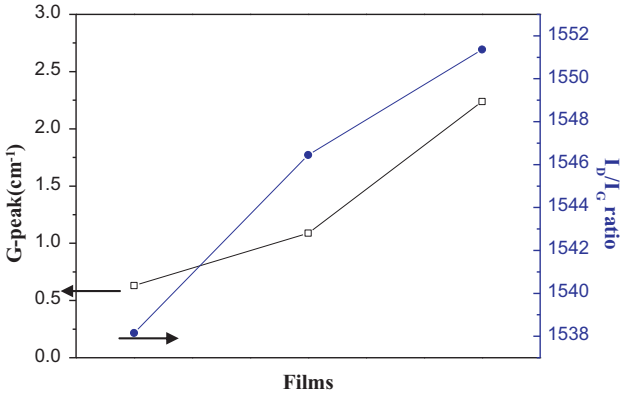

Fig. 4. Corresponding G peak position and I_D/I_G obtained from the Raman spectra. (For interpretation of the references to color in figure legend, the reader is referred to the web version of the article.)

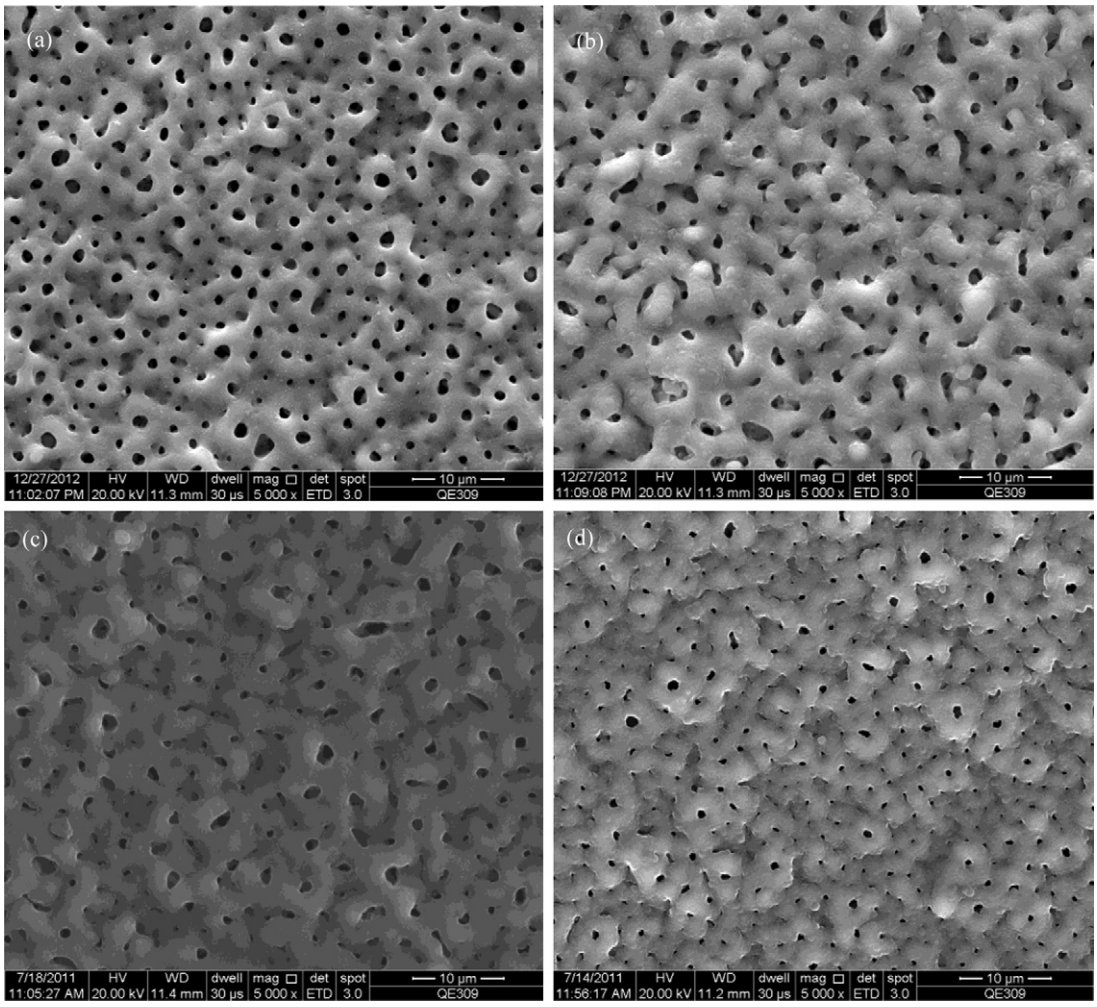

Fig. 5. Surface morphologies of the coatings, (a) MAO, (b) DLC/MAO, (c) Ti-DLC/MAO and (d) (Ti:N)-DLC/MAO.

3.2. Tribological properties

Fig. 7 presents the friction coefficient of the four coated AZ80 magnesium alloy against sliding distance. For the MAO coated sample, the frictional coefficient jumped to 0.5 within the first few sliding cycles and then the friction coefficient remained stable during the whole wear test. The MAO coating was completely worn off from the Mg alloy substrate during friction measurement. The deposition of DLC film onto the MAO coating improved the dry friction behavior significantly and the friction coefficient of duplex DLC/MAO coating was nearly kept about 0.2 during the

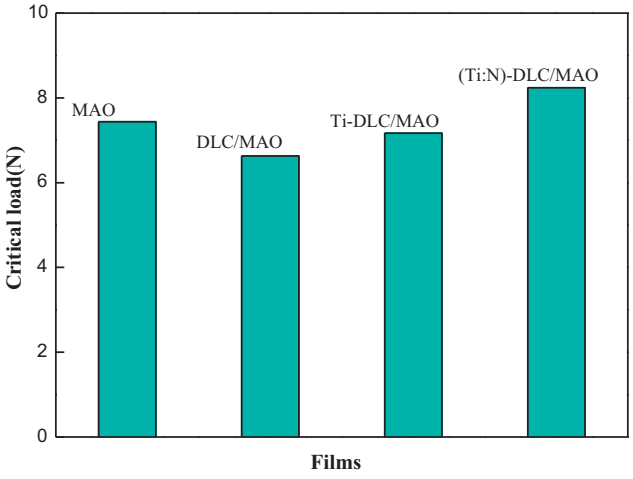

Fig. 6. Critical load of MAO, DLC/MAO, Ti-DLC/MAO and (Ti:N)-DLC/MAO coatings on AZ80 Mg alloy.

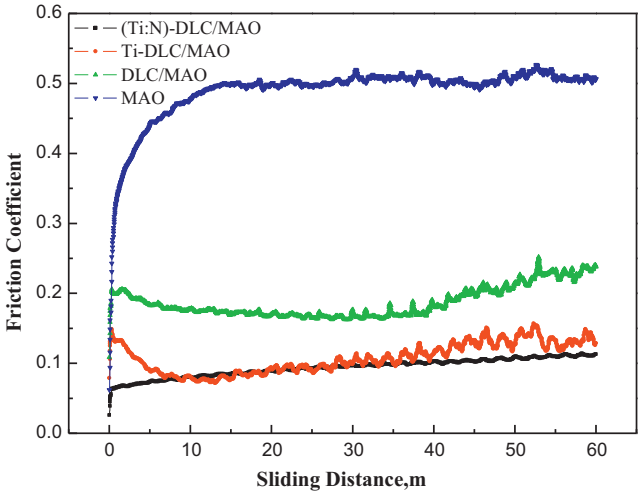

Fig. 7. Coefficient of friction (COF) of the films coating AZ80 as a function of sliding distance.

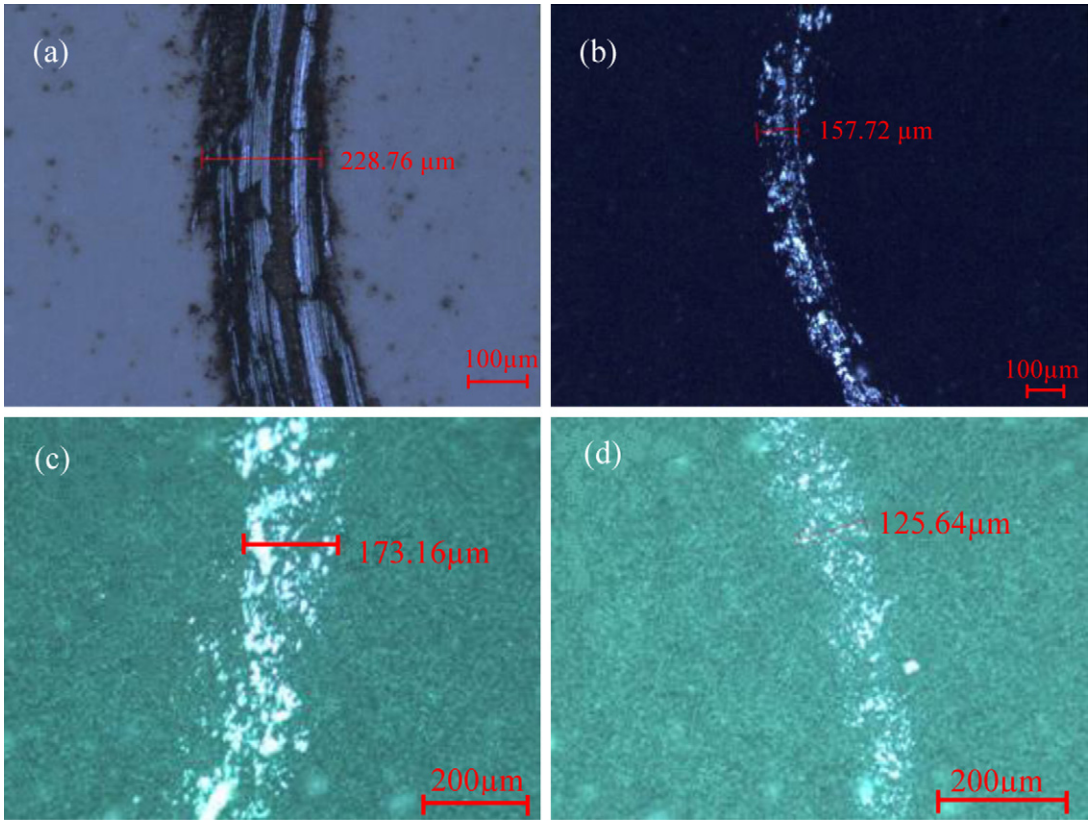

Fig. 8. OM images of the wear scar of the coatings, (a) MAO, (b) DLC/MAO, (c) Ti-DLC/MAO and (d) (Ti:N)-DLC/MAO.

overall sliding test. Interestingly, the friction coefficient increased as the sliding distance after 30 m, which could be deduced that the increased debris, generated from the DLC film as the lubrication media between the duplex DLC/MAO coating and steel ball, may result in the increased friction coefficient. In the case of the duplex (Ti:N)-DLC/MAO coating, It can be seen that the friction coefficient reached a stable value of 0.1. Previous studies on tribological behaviors of DLC films conformed that the low friction coefficient could be attributed to graphitization induced by localized rising temperature at asperity contacts [34]. From the Raman analysis, the fraction of sp^2 carbon bonds of (Ti:N)-DLC top film increased, compared with the DLC and Ti-DLC films, which indicated that graphitization trend also increased. So this duplex coating exhibits an excellent lubricating property with low steady-state friction coefficient. Since the duplex Ti-DLC/MAO coating showed a low but not-stable friction coefficient, there must be a self-lubricating mechanism for the microstructure of duplex (Ti:N)-DLC/MAO coating in dry friction to improve the tribological property. Moreover, the high binding strength of duplex (Ti:N)-DLC/MAO is also useful to improve the tribological behavior.

To investigate the tribological behavior of the obtained coatings on the AZ80 substrate, the OM morphology was used to obtain the wear scar and debris composition of the films after friction tests. Fig. 8 shows the width of the wear scar, and the partially elaborated chemical composition by EDS is shown in the Table 2. The results show that the width of wear scars of MAO/AZ80, DLC/MAO/AZ80 and Ti-DLC/MAO/AZ80 and (Ti:N)-DLC/MAO/AZ80 coated samples is 228.76 μm, 157.72 μm, 173.16 μm, and 125.64 μm, respectively. It is observed that the wear scar of MAO coated Mg alloy substrate is broad and deep, and the Mg substrate has been exposed. As a consequence, the sudden increase of the friction coefficient on the MAO coating mainly attributes to the destroyed films. It is confirmed that a large number of Fe and O are detected from the wear trace of the MAO coated substrate. This reveals that the formation of oxide due to the temperature spikes occurs at asperity contacts between the counter-body steel ball and the film during the friction [19]. The wear tracks of the DLC/MAO and Ti-DLC/MAO coated AZ80 Mg alloy are much shallower and narrower than that of the MAO coated sample. Obviously, the (Ti:N)-DLC/MAO coated AZ80 Mg alloy shows the best wear resistance. It is noted that the detected C element on the wear tracks of the duplex DLC/MAO, Ti-DLC/MAO and (Ti:N)-DLC/MAO coatings denotes that the duplex coatings are survived during all the sliding. In other aspect, much less of O is detected on the wear tracks of the three duplex coatings, which indicates that high-temperature oxidation process during the sliding process is observably restrained. In conclusion, the duplex (Ti:N)-DLC/MAO coating could greatly improve the wear resistance of the AZ80 Mg alloy in this study.

Table 2
Composition at wear tracks of the films in Fig. 8.

Sample	C	O	Fe	Ti	Si	Mg	Al
MAO/AZ80		57.15	35.98		1.83	4.20	0.83
DLC/MAO/AZ80	87.73	5.57	0.26		1.36	4.68	0.41
Ti-DLC/MAO/AZ80	80.20	11.40	1.70		1.53	3.60	1.57
(Ti:N)-DLC/MAO/AZ80	84.15	4.43	0.58	3.18	1.91	3.31	2.44

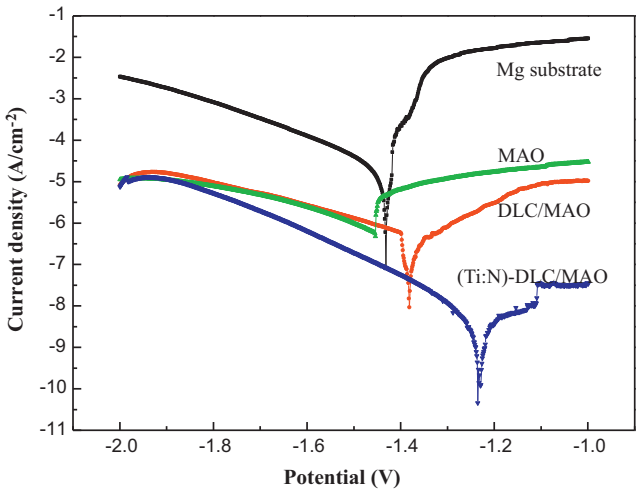

Fig. 9. Polarization curves of Mg substrate and MAO, DLC/MAO, (Ti:N)-DLC/MAO coatings on AZ80 Mg alloy.

3.3. Corrosion resistance

The polarization curves of the coated AZ80 Mg alloy in the 3.5 wt.% NaCl solution are shown in Fig. 9. Corrosion potential and corrosion current density obtained from Fig. 9 by Tafel analysis are shown in Table 3. Based on these electrochemical parameters, it is known that the corrosion current density of the duplex (Ti:N)-DLC/MAO coating decreased to 5.0508×10^{-9} A/cm^2, which is much lower than that of the duplex DLC/MAO coating (2.135×10^{-7} A/cm^2) and the MAO monolayer (2.002×10^{-6} A/cm^2). It indicates that the corrosion resistance of the AZ80 Mg alloy substrate is improved significantly by the duplex (Ti:N)-DLC/MAO coating in the 3.5 wt.% NaCl solution.

Table 3
Corrosion current density and potential of the four films in Fig. 9.

Films	Corrosion current density (A/cm^{-2})	Corrosion potential (V)
Mg substrate	5.159E−5	−1.432
MAO/AZ80	2.002E−6	−1.458
DLC/MAO/AZ80	2.135E−7	−1.287
(Ti:N)-DLC/MAO/AZ80	5.508E−9	−1.251

Fig. 10 shows the surface morphologies of the four coatings after corrosion test. It is observed that the AZ80 Mg alloy substrate is completely destroyed in corrosion test, and some corrosion products and cracks appear on the substrate surface. For the MAO coating, a local region is suffered from accelerated corrosion due to the micropores, but the Mg alloy substrate is still protected by the MAO coating. It is also seen that a large number of micropores of MAO coating have been sealed by the corrosion products, which is useful to restrain the corrosion process. In the case of DLC/MAO coating, the surface morphology is also changed and some large corrosion pits are observed on the surface. Because there are still some micropores on the duplex coating surface, even in good quality PVD or CVD DLC films, some regions of the MAO interlayer could be exposed to the corrosive environment, which results in

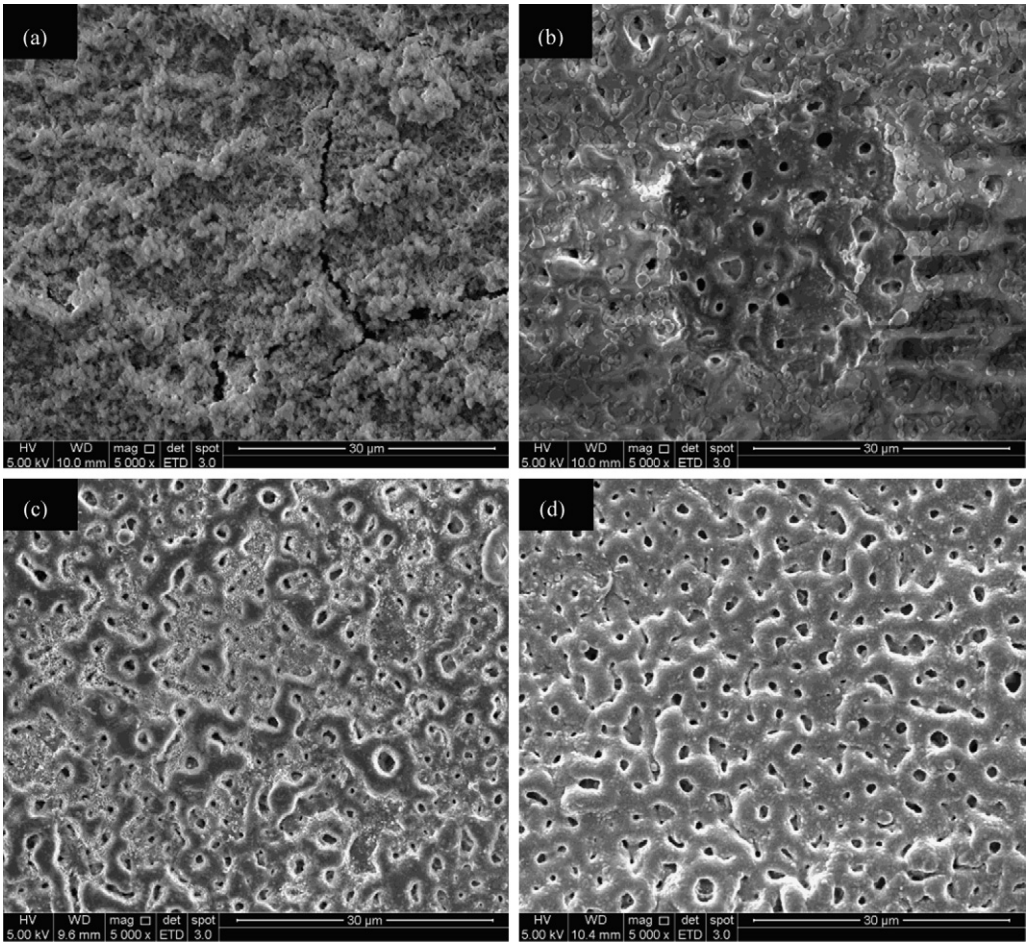

Fig. 10. Surface micrograph of the AZ80 substrate (a) and the substrate coated by (b) MAO, (c) DLC/MAO and (d) (Ti:N)-DLC/MAO after corrosion test.

the corrosion of DLC/MAO coating. The surface feature of (Ti:N)-DLC/MAO coating is not changed after the corrosion test, which illustrates that the anti-corrosion property is strongly improved by this duplex coating. It is convincing that the formation of galvanic cell between the MAO interlayer and substrate, resulted in the corrosive occurrence, was largely restrained by the top (Ti:N)-DLC film.

4. Conclusions

The duplex (Ti:N)-DLC/MAO coating was successfully fabricated on AZ80 magnesium alloy using MAO as pretreatment to improve the properties of the substrate. In this work, it was determined that (Ti:N)-DLC top film with TiN crystalline phase was obtained on the MAO coating surface, which owned the increased sp^2/sp^3 ratio compared with the DLC and Ti-DLC films. The (Ti:N)-DLC top film was very useful to increase the binding strength between the coating and Mg alloy substrate. As a result, The coated Mg alloy sample showed significantly improved wear resistance and corrosion resistance for the special microstructure of (Ti:N)-DLC/MAO coating.

Acknowledgments

The authors gratefully acknowledge the financial support of the Natural Science Foundation of China (Grant No. 51201176), Ningbo Municipal Nature Science Foundation (Grant No. 201101A6105005) and Major projects of Department of Science and Technology of Zhejiang Province (2010C13025-1).

References

[1] T.N. Kim, Q.L. Feng, Z.S. Luo, F.Z. Cui, J.O. Kim, Surface and Coatings Technology 9 (1998) 20.
[2] J.E. Gray, B. Luan, Journal of Alloys and Compounds 336 (2002) 88.
[3] A.L. Yerokhin, A. Voevodin, V. Lyubimov, J. Zabinski, M. Donley, Surface and Coatings Technology 110 (1998) 140.
[4] L. Wen, Y.M. Wang, Y. Zhou, L.X. Guo, J.H. Ouyang, Corrosion Science 53 (2011) 473.
[5] Y.M. Wang, T.Q. Lei, B.L. Jiang, L.X. Guo, Applied Surface Science 233 (2004) 258.
[6] W.B. Xue, Z.W. Deng, Y.C. Lai, R.Y. Chen, Journal of the American Ceramic Society 81 (1998) 1365.
[7] V.N. Malyshev, K.M. Zorin, Applied Surface Science 254 (2007) 1511.
[8] J.Z. Li, Y.W. Tian, Z.X. Cui, Rare Metal Materials and Engineering 36 (2007) 528.
[9] Y.M. Wang, B.L. Jiang, T.Q. Lei, L.X. Guo, Applied Surface Science 246 (2005) 214.
[10] P. Shi, W.F. Ng, M.H. Wong, F.T. Cheng, Journal of Alloys and Compounds 469 (2009) 286.
[11] J. Choi, S. Nakao, J. Kim, M. Ikeyama, T. Kato, Diamond and Related Materials 16 (2007) 1361.
[12] H. Mohrbacher, J.P. Celis, Diamond and Related Materials 4 (1995) 1267.
[13] A.Y. Wang, H.S. Ahn, K.R. Lee, J.P. Ahn, Applied Physics Letters 86 (2005) 111902.
[14] A.Y. Wang, K.R. Lee, J.P. Ahn, J.H. Han, Carbon 44 (2006) 1826–1832.
[15] W. Dai, A.Y. Wang, Journal of Alloys and Compounds 509 (2011) 4626–4631.
[16] G. Capote, L.F. Bonetti, L.V. Santos, V.J. Trava-Airoldi, E.J. Corat, Thin Solid Films 516 (2008) 4011.
[17] Y.S. Li, Y. Tang, Q. Yang, C. Xiao, A. Hirose, Applied Surface Science 256 (2010) 7653.
[18] G.A. Zhang, P.X. Yan, P. Wang, Y.M. Chen, J.Y. Zhang, L.P. Wang, J.Y. Zhang, Surface and Coatings Technology 202 (2008) 2684.
[19] Y.H. Lin, H.D. Lin, C.K. Liu, M.W. Huang, J.R. Chen, H.C. Shih, Diamond and Related Materials 19 (2010) 1034.
[20] G.S. Wu, W. Dai, H. Zheng, A.Y. Wang, Surface and Coatings Technology 205 (2010) 2067.
[21] W. Dai, G.S. Wu, A.Y. Wang, Diamond and Related Materials 19 (2010) 1307.
[22] G.S. Wu, L.L. Sun, W. Dai, L.X. Song, A.Y. Wang, Surface and Coatings Technology 257 (2011) 4699.
[23] W. Yang, A.Y. Wang, P.L. Ke, B.L. Jiang, Acta Metallurgica Sinica 47 (2011) 1535.
[24] H.K. Li, Q. Liu, G.Q. Lin, C. Dong, Acta Metallurgica Sinica 45 (2009) 610.
[25] W. Dai, H. Zheng, G. Wu, A. Wang, Vacuum 85 (2010) 231.
[26] T.W. Scharf, R.D. Ott, D. Yang, J.A. Barnard, Journal of Applied Physics 85 (1999) 3142.
[27] E. Riedo, F. Comin, J. Chevrier, F. Schmithusen, S. Decossas, M. Sancrotti, Surface and Coatings Technology 125 (2000) 124.
[28] V. Chawla, R. Jayaganthan, Ramesh Chandra, Materials Characterization 59 (2008) 1015.
[29] M.V. Gradowski, A.C. Ferrari, R. Ohr, B. Jacoby, H. Hilgers, H.H. Schneider, H. Adrian, Surface and Coatings Technology 174 (2003) 246.
[30] W.G. Cui, Q.B. Lai, L. Zhang, F.M. Wang, Surface and Coatings Technology 205 (2010) 1995–1999.
[31] C. Casiraghi, A.C. Ferrari, J. Robertson, Physical Review B 72 (2005) 085401.
[32] Y. Tang, Y.S. Li, Q. Yang, A. Hirose, Applied Surface Science 256 (2010) 7653.
[33] J.F. Cui, L. Qiang, B. Zhang, X. Ling, Tao Yang, J.Y. Zhang, Applied Surface Science 258 (2012) 5025.
[34] W.J. Hsieh, C.C. Lin, U.S. Chen, Y.S. Chang, H.C. Shih, Diamond and Related Materials 14 (2005) 93.